Influence of inertia on viscous fingering patterns: Rectangular and radial flows

Eduardo O. Dias and José A. Miranda*
Departamento de Física, Universidade Federal de Pernambuco, Recife, PE 50670-901, Brazil
(Received 18 March 2011; published 17 June 2011)

Recently, there has been a growing interest in the impact of inertial effects on the development of the Saffman-Taylor instability. Experiments and theory indicate that inertia may have a significant influence on the system's behavior. We employ a perturbative-mode-coupling method to examine how the stability and morphology of the viscosity-driven fingering patterns are affected by inertia. Both rectangular and radial Hele-Shaw flow geometries are considered. In the rectangular configuration useful results can be deduced analytically, and in closed form. In particular, we have found that inertia has a stabilizing role at the linear stage, and tends to widen the fingers at the weakly nonlinear regime. These analytical results are consistent with existing experimental findings. The analysis of the system is not as simple in radial flow geometry, but it still allows the capture of inertially induced, enhanced finger tip splitting events at the onset of nonlinearities.

DOI: 10.1103/PhysRevE.83.066312 PACS number(s): 47.54.−r, 47.20.Gv, 47.15.gp, 47.15.km

I. INTRODUCTION

The Saffman-Taylor problem [1] is one of the most studied among fluid dynamic systems presenting formation and evolution of patterned structures. It considers the development of interfacial instabilities when a fluid displaces another of higher viscosity between the narrowly spaced plates of a Hele-Shaw cell [2]. The problem is traditionally studied in two basic Hele-Shaw cell geometries, respectively, rectangular [1,3–8] (longitudinal flow in a rectangular channel), or radial [9–14] (axisymmetric fluid injection). Radial geometry exhibits branched morphologies markedly characterized by the spreading, and subsequent splitting of the growing fingers. Conversely, flow in the rectangular configuration normally displays fingers that do not tend to bifurcate. Commonly, the system evolves until a single stable finger forms.

A large body of theoretical and experimental work on the Saffman-Taylor instability addresses flow in very thin cell gaps, and considers that the displaced fluid is highly viscous, so that inertial effects can be safely neglected. This characterizes a vanishing Reynolds number flow described by the usual Darcy's law [1–14]. Nevertheless, the quest for even richer dynamic behavior, and the desire to understand how inertia could alter the shape of the patterns motivated some research groups to revisit the classic viscous fingering problem [15–20]. They focused on situations in which inertia could play a relevant role by utilizing displaced fluids of low viscosity, larger plate spacings, and larger flow speeds. In this context, the governing hydrodynamic equation is a modified, effectively two-dimensional (2D) Darcy's law based on a gap-averaging process of the 3D Navier-Stokes equation which includes the contribution of inertial terms.

An interesting example of the emergence of important inertial effects in rectangular Hele-Shaw flow has been recently studied experimentally in Ref. [18]. It has been found that, contrary to the conventional noninertial behavior, one observes an increase in the finger width for high-flow speeds. It turns out this distinct finger broadening effect is induced by inertia. Besides, inertial corrections to the radial Hele-Shaw problem have been theoretically examined in the zero-surface-tension limit [19]. A linear stability analysis of this idealized system suggests that inertia tends to stabilize interfacial disturbances. Another recent theoretical investigation revealed that inertia affects both the stability and shape of patterns produced by centrifugally driven Hele-Shaw flows [20].

So, regarding the effect of inertia on viscosity-driven instabilities in Hele-Shaw cells, previous works examined *experiments* in rectangular configuration, and *purely linear* analysis (in the zero-surface-tension limit) for radial displacements. Despite the significance and usefulness of these particular efforts, a theoretical study about the influence of inertia on the morphology of injection-induced radial fingering patterns, as well as its action on the finger widening phenomenon detected in rectangular geometry still need to be performed. These important nonlinear issues can be addressed by a perturbative weakly nonlinear approach. That is precisely what we intend to do in this work.

In this paper we tackle both rectangular and radial geometry Hele-Shaw problems, and investigate the role played by inertia in determining key features of the pattern-forming dynamics. This is done by employing a mode-coupling theory, and assuming the presence of realistic nonzero surface tension effects. We find that the rectangular flow problem is particularly well suited to analytical treatment, permitting a simplified description of important stability and morphological aspects during linear and early nonlinear flow stages. Unfortunately, it is difficult to formulate a closed form, purely analytical portrayal of inertial effects in the radial Hele-Shaw situation. Even so, mode coupling still allows one to gain insight into relevant aspects of radial flow patterns, such as finger tip splitting.

The layout of the rest of the paper is as follows. Section II presents the derivation of the weakly nonlinear equations for Hele-Shaw flows in rectangular geometry when inertial effects are taken into account. A linear stability analysis of the rectangular case is performed in Sec. II B. Useful analytical information about the influence of inertia on the width of the fingers is discussed in Sec. II C. The analysis of the radial geometry flow is carried out in Sec. III, where we focus on the impact of inertia on the important mechanism of finger tip splitting. Our main results and conclusions are summarized in Sec. IV.

*jme@df.ufpe.br

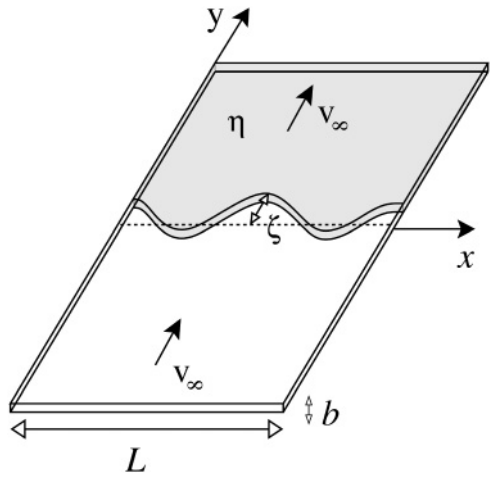

FIG. 1. Schematic representation of the rectangular Hele-Shaw flow setup.

II. EFFECT OF INERTIA: RECTANGULAR GEOMETRY

A. Mode-coupling differential equation

Consider two semi-infinite immiscible fluids, flowing in a narrow gap of thickness b, between two parallel plates of a rectangular Hele-Shaw cell. The cell lies in the x-y plane (Fig. 1). The displacing fluid has negligible viscosity, while the displaced fluid has viscosity η. Between the two fluids there exists a surface tension σ. The inviscid fluid is injected at constant external flow velocity $\mathbf{v}_\infty = v_\infty \hat{\mathbf{y}}$ at $y = -\infty$ and withdraws the viscous fluid at the same velocity at $y = +\infty$. Here $\hat{\mathbf{y}}$ denotes the unit vector along the y axis. We describe the system in a frame moving with velocity $\mathbf{v}_\infty$, so that the interface may deform, but it does not displace from $y = 0$ (dashed line in Fig. 1) on the average.

During the flow, the interface has a perturbed shape described in the form of a Fourier series $y = \zeta(x,t) = \sum_k \zeta_k(t)\exp(ikx)$ over the range $0 \leqslant x \leqslant L$ in the comoving frame, where $\zeta_k(t)$ denotes the complex Fourier mode amplitudes. The wave vectors k are constrained to lie on the x axis, but can be either positive or negative. Note that the $k = 0$ mode vanishes since we are in a comoving frame. Periodic boundary conditions are applied along the x axis so that $k = 2\pi n/L$, for integer n. The analytic model we employ [8] keeps up to second-order terms in ζ, and describes the linear and early nonlinear dynamics of the system.

In order to investigate the influence of inertia on the Saffman-Taylor instability we follow the theoretical approach originally developed in Refs. [15–20], and consider that the fluid flow is governed by a gap-averaged nonlinear generalized Darcy's law equation

$$\rho\left[\frac{\partial \mathbf{u}}{\partial t} + \frac{6}{5}(\mathbf{u}\cdot\nabla)\mathbf{u}\right] = -\nabla p - \frac{12\eta}{b^2}\mathbf{u}, \tag{1}$$

and by a 2D continuity equation for an incompressible fluid

$$\nabla \cdot \mathbf{u} = 0. \tag{2}$$

Here $\mathbf{u} = \mathbf{v} + \mathbf{v}_\infty$, where $\mathbf{v} = v_x\hat{\mathbf{x}} + v_y\hat{\mathbf{y}}$ denotes the velocity with respect to the comoving frame, and p is the hydrodynamic pressure. The coefficients appearing in front of the terms $\partial\mathbf{u}/\partial t$ and $(\mathbf{u}\cdot\nabla)\mathbf{u}$ may vary depending on the way the gap averaging is performed, but are always of order 1. By taking into consideration the potential nature of the flow [18,19], Eq. (1) can be conveniently rewritten in a *dimensionless* form as

$$\mathrm{Re}\left[\frac{\partial\phi}{\partial t} - \frac{3}{5}|\nabla\phi|^2\right] = p - \phi, \tag{3}$$

where ϕ ($\mathbf{u} = -\nabla\phi$) is a velocity potential. The parameter

$$\mathrm{Re} = \frac{\rho U b^2}{12\eta L} \tag{4}$$

defines a Reynolds number that quantifies the effect of inertia on the system. In Eq. (3) lengths and velocities are rescaled by L, and by a characteristic velocity $U = v_\infty$, respectively. From this point on, we work with the dimensionless version of the equations.

Due to surface tension the pressure satisfies a Young-Laplace boundary condition [2], which expresses the pressure jump across the fluid-fluid interface

$$p = B\kappa, \tag{5}$$

where the in-plane interfacial curvature is denoted by κ, and

$$B = \frac{\sigma b^2}{12\eta U L^2} \tag{6}$$

represents an effective surface tension parameter. The problem is specified by Eq. (5), augmented with the kinematic boundary condition

$$\frac{\partial\zeta}{\partial t} = \left(v_y - v_x\frac{\partial\zeta}{\partial x}\right)_{y=\zeta}, \tag{7}$$

which states that the interface moves according to the local fluid velocities.

Considering the incompressibility condition (2), we define Fourier expansions for the velocity potential, which obeys Laplace's equation $\nabla^2\phi = 0$. Then, we write ϕ in terms of the perturbation amplitudes ζ_n by considering condition (7). Substituting these relations, and the pressure jump condition (5) into Eq. (3), always keeping terms up to second order in ζ, and Fourier transforming, we find the equation of motion for the perturbation amplitudes in rectangular geometry (for $k \neq 0$)

$$\begin{aligned}\mathrm{Re}\ddot{\zeta}_k + \left(1 - \mathrm{Re}\frac{|k|}{5}\right)\dot{\zeta}_k - \Lambda(k)\zeta_k \\ = \sum_{k'\neq 0}[G(k,k') + \mathrm{Re}I(k,k')]\dot{\zeta}_{k'}\zeta_{k-k'} \\ + \mathrm{Re}\sum_{k'\neq 0}[G(k,k')\ddot{\zeta}_{k'}\zeta_{k-k'} + J(k,k')\dot{\zeta}_{k'}\dot{\zeta}_{k-k'}],\end{aligned} \tag{8}$$

where the overdot denotes total time derivative, and $\Lambda(k) = |k|[1 - Bk^2]$. The mode coupling terms are given by

$$G(k,k') = |k|[1 - \mathrm{sgn}(kk')], \tag{9}$$

$$I(k,k') = \frac{|k|}{5}[|k|\mathrm{sgn}(kk') - |k'|], \tag{10}$$

and

$$J(k,k') = |k| \left\{ \frac{3}{5}[1 - \mathrm{sgn}(k'(k-k'))] - \mathrm{sgn}(kk') \right\}. \quad (11)$$

The sgn function equals ± 1 according to the sign of its argument. Equations (8)–(11) constitute one of the principal results of this work, yielding the time evolution of the perturbation amplitudes accurate to second order, including the action of inertial effects. Notice that when Re = 0 Eq. (8) reproduces the simpler results obtained in Ref. [8] for the corresponding problem without inertia.

While presenting our results in Secs. II B and II C we make sure that the values of the relevant dimensionless quantities Re and B are consistent with realistic physical parameters related to existing experimental arrangements, and material properties of the fluids [18]. This is also true for the results presented in Sec. III for the radial flow problem [9–11].

B. Linear stability analysis

At the linear level Eq. (8) is significantly simplified yielding a second-order ordinary differential equation with constant (in time) coefficients

$$\mathrm{Re}\ddot{\zeta}_k + \left(1 - \mathrm{Re}\frac{|k|}{5}\right)\dot{\zeta}_k - \Lambda(k)\zeta_k = 0. \quad (12)$$

By setting $\zeta_k(t=0) = \zeta_k(0)$, and $\dot{\zeta}_k(t=0) = 0$ the linear solution can be written in closed form as

$$\zeta_k(t) = \frac{\zeta_k(0)}{\lambda_- - \lambda_+}[\lambda_- \exp(\lambda_+ t) - \lambda_+ \exp(\lambda_- t)], \quad (13)$$

where

$$\lambda_\pm = \frac{1}{2\mathrm{Re}}\left[\pm \sqrt{\left(1 - \mathrm{Re}\frac{|k|}{5}\right)^2 + 4\mathrm{Re}\Lambda(k)} - \left(1 - \mathrm{Re}\frac{|k|}{5}\right)\right]. \quad (14)$$

For experimental situations of interest [18] the term involving $\exp(\lambda_- t)$ drops off very quickly. So, after a very short transient, the linear solution can be accurately rewritten in a simpler form

$$\zeta_k(t) = \zeta_k(0)\left[\frac{\left(1 - \mathrm{Re}\frac{|k|}{5}\right) + \mathrm{Re}\lambda(k)}{\left(1 - \mathrm{Re}\frac{|k|}{5}\right) + 2\mathrm{Re}\lambda(k)}\right]\exp[\lambda(k)t], \quad (15)$$

where $\lambda(k) = \lambda_+$ denotes the linear growth rate. We point out that oscillatory solutions of Eq. (12) fall off exponentially with time. We can see that in the limit $\mathrm{Re} \to 0$, $\lambda(k) \to \Lambda(k)$, i.e., we recover the growth rate expression obtained for the noninertial problem [8].

The critical wave number separating unstable from stable regions is obtained by the condition $\lambda(k) = 0$, yielding

$$k_c = \frac{1}{\sqrt{B}}. \quad (16)$$

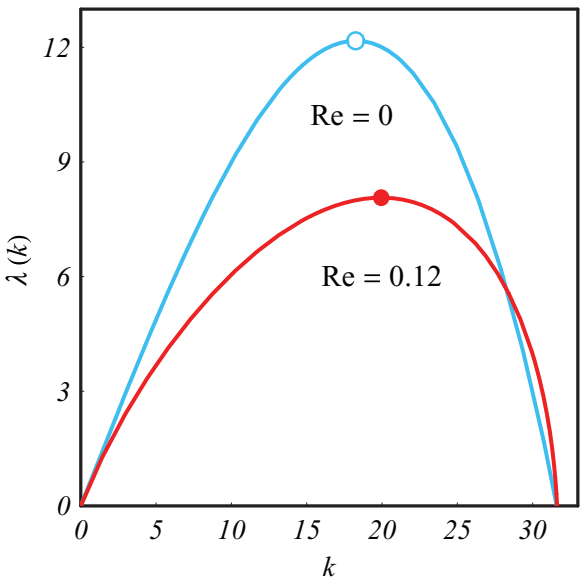

FIG. 2. (Color online) Linear growth rate $\lambda(k)$ as a function of k, for Re = 0, Re = 0.12, and $B = 0.001$. The maxima of the curves are indicated by small circles.

It defines the width of the band of unstable modes, and is independent of the controlling parameter Re. While k_c is not modified by inertia, the fastest growing mode [obtained by setting $d\lambda(k)/dk$=0] has a complicated dependence on the Reynolds number, being a solution of a quartic algebraic equation in k. But in the lowest order correction in Re the mode of maximum growth rate simplifies to

$$k_{\max} \approx k^{\mathrm{o}}_{\max}\left(1 + \frac{k^{\mathrm{o}}_{\max}}{15}\mathrm{Re}\right), \quad (17)$$

where $k^{\mathrm{o}}_{max} = 1/\sqrt{3B}$ is the fastest growing mode when inertia is neglected.

Figure 2 plots $\lambda(k)$ as a function of wave number k for two values of Re: 0 and 0.12, and for $B = 0.001$. First, it is evident that the band of unstable modes is not modified as the Reynolds number is changed. However, it is also clear that there is a considerable decrease in the magnitude of the growth rate of the wave number of maximum growth when inertial effects are taken into account. This characterizes a stabilizing role of the inertial effects in rectangular geometry. In addition, it can also be observed that the position of the wave number of maximum growth is shifted toward higher values of k for a nonzero Re. This wavelength selection at the linear regime, which results from the action of inertia, sort of encourages the idea that inertia could lead to enhanced tendency toward finger broadening at subsequent stages of the dynamics. The correctness of this a bit conjectural linear prediction will be checked by our early nonlinear analysis.

C. Weakly nonlinear analysis

To establish a better connection with the weakly nonlinear results originally obtained in Ref. [8] for the noninertial situation, we begin by performing a small manipulation in the mode-coupling equation (8). From the simplicity of the linear solution (15), we can write that $\dot{\zeta}_k = \lambda(k)\zeta_k$ [20]. Therefore,

Eq. (8) can be suitably written as a first-order (in time) differential equation

$$\dot{\zeta}_k = \lambda(k)\zeta_k + \sum_{k'\neq 0} Y(k,k')\zeta_{k'}\zeta_{k-k'}, \tag{18}$$

where

$$Y(k,k') = \frac{\lambda(k')\{G + \mathrm{Re}[I + \lambda(k')G + \lambda(k-k')J]\}}{1 + \mathrm{Re}\left[\lambda(k) + \lambda(k') + \lambda(k-k') - \frac{|k|}{5}\right]} \tag{19}$$

is obtained by substituting Eq. (18) into Eq. (8), and keeping consistent second-order expressions involving the perturbation amplitudes. In Eq. (19) G, I, and J are the functions presented in Eqs. (9)–(11), respectively. We call attention to the fact that when $\mathrm{Re} = 0$, Eq. (18) reproduces the second order form of the mode coupling equation originally derived in Ref. [8]. It is beneficial to recast Eq. (8) as Eq. (18) since this is exactly the form which allows one to gain insight about morphological aspects of the interface in a fairly simple fashion.

To get useful analytical information about the problem, as in Refs. [8,12], we advance by considering the coupling of a small number of modes. Our discussion is simplified further by rewriting Eq. (18) in terms of cosine and sine modes, where the cosine $a_k = \zeta_k + \zeta_{-k}$ and sine $b_k = i\,(\zeta_k - \zeta_{-k})$ amplitudes are real valued. Without loss of generality we choose the phase of the fundamental mode so that $a_k > 0$ and $b_k = 0$. The finger tip behavior (tip widening and tip narrowing phenomena) is related to the influence of a fundamental mode k [assuming that $\lambda(2k) = 0$] on the growth of its harmonic $2k$ [8]. The equations of motion for the harmonic mode are written as

$$\dot{a}_{2k} = \lambda(2k)a_{2k} + \tfrac{1}{2}T(2k,k)a_k^2, \tag{20}$$

$$\dot{b}_{2k} = \lambda(2k)b_{2k}, \tag{21}$$

where a generalized finger tip function (including inertial effects)

$$T(2k,k) = Y(2k,k), \tag{22}$$

controls the appearance of the finger. From Eq. (21) it is obvious that there is no second-order coupling for the sine harmonic mode. The sign of $T(2k,k)$ dictates whether finger tip widening or finger tip narrowing is favored by the dynamics. If $T(2k,k) < 0$, the result is a driving term of order a_k^2 forcing growth of $a_{2k} < 0$, the sign that is required to cause fingers to get wider. By contrast, if $T(2k,k) > 0$ growth of $a_{2k} > 0$ would be favored, leading to finger tip narrowing. It is important to note that when $\mathrm{Re} = 0$ the finger tip function vanishes, meaning that there is no second-order coupling at all when inertia is absent. Hence, if inertial effects are neglected one cannot detect any sign of finger broadening behavior at second order in rectangular flow geometry.

Figure 3 illustrates how the finger tip function $T(2k,k)$ is changed as Re is increased. The solid (dashed) curve considers that $B = 0.001$ ($B = 0.003$). First, as expected, when $\mathrm{Re} = 0$ the finger tip function is indeed zero. For a given B we see that increasingly larger values of Re lead to more negative values of $T(2k,k)$. Therefore, inertial effects tend to favor the broadening of the fingers. Additionally, one can see that such a behavior is more intense for smaller values of B. We emphasize that these theoretical findings are consistent with the experimental results observed in Ref. [18].

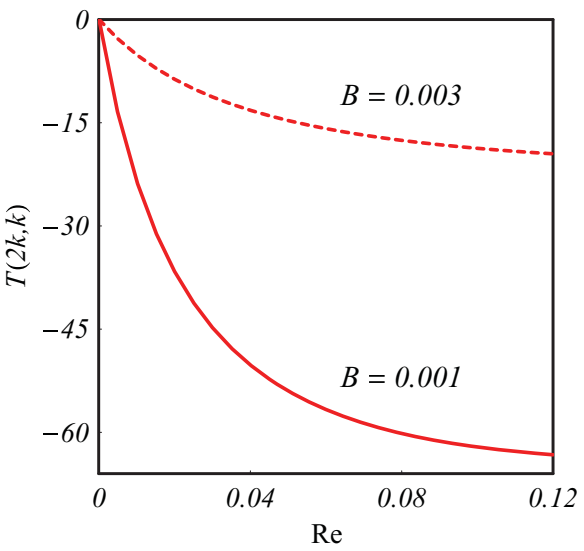

FIG. 3. (Color online) $T(2k,k)$ as a function of Re, for two different values of B: 0.001 (solid curve) and 0.003 (dashed curve).

It is worth noting that in Fig. 3 we are able to fix the value of B while the Reynolds number is increased. However, in the experiments performed in Ref. [18] the main tuning parameter is the flow velocity U, so that by changing U both B and Re are simultaneously modified. This would imply in an interplay between these two parameters in determining the finger broadening behavior. But, in the end, both in this work and in [18] the net effect of inertia is to widen the fingers.

III. EFFECT OF INERTIA: RADIAL GEOMETRY

In this section we turn to the investigation of the role played by inertia on the Saffman-Taylor problem in radial geometry. We do that by focusing on the influence of inertial effects on the most celebrated morphological feature in radial Hele-Shaw flows: the finger tip splitting phenomenon. To study this interfacial behavior we must go beyond purely linear stages, and access the early nonlinear dynamics of the system.

Similarly to what we have done in Sec. II A, we consider a Hele-Shaw cell of spacing b initially containing a viscous incompressible fluid of viscosity η and density ρ. Then, another fluid of negligible density and viscosity is injected into the viscous fluid at a constant injection rate Q, equal to the area covered per unit time (see Fig. 4). Between the two fluids there exists a surface tension σ. The perturbed fluid-fluid interface is described as $\mathcal{R}(\theta,t) = R(t) + \zeta(\theta,t)$, where θ represents the azimuthal angle, and $R(t)$ is the time dependent unperturbed radius $R = R(t) = \sqrt{R_0{}^2 + Qt/\pi}$, with R_0 being the unperturbed radius at $t = 0$. In addition, $\zeta(\theta,t) = \sum_{n=-\infty}^{+\infty} \zeta_n(t)\exp(in\theta)$ denotes the net interface perturbation with Fourier amplitudes $\zeta_n(t)$, and discrete azimuthal wave numbers n. As in Sec. II our perturbative approach keeps terms up to the second order in ζ. In the Fourier expansion of ζ we include the $n = 0$ mode to maintain the area of the perturbed shape independent of the perturbation ζ. Mass conservation

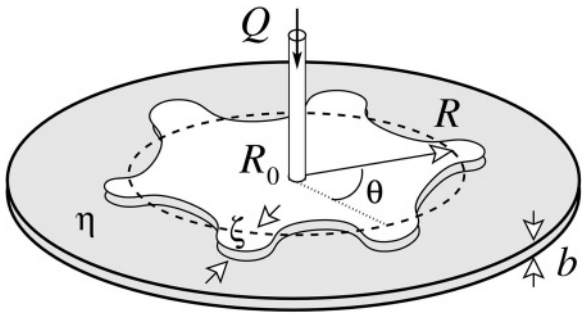

FIG. 4. Schematic representation of the radial Hele-Shaw flow setup.

imposes that the zeroth mode is written in terms of the other modes as $\zeta_0 = -(1/2R)\sum_{n\neq 0}|\zeta_n(t)|^2$.

By utilizing the generalized Darcy's law (3), the relevant boundary conditions [Eqs. (5) and (7)], and by following the same basic steps described in Sec. II, we obtain the second-order mode-coupling dimensionless equation for the radial flow geometry (with $n \neq 0$)

$$\begin{aligned}
&\mathrm{Re}\ddot{\zeta}_n + \left[1 - \mathrm{Re}\frac{\dot{R}}{R}\left(\frac{|n|}{5} - 2\right)\right]\dot{\zeta}_n \\
&\quad - \left[\Lambda(n) - \mathrm{Re}\frac{\dot{R}^2}{R^2}(|n| - 1)\right]\zeta_n \\
&\qquad = \sum_{n'\neq 0}[\mathcal{F}(n,n') + \mathrm{Re}\mathcal{H}(n,n')]\zeta_{n'}\zeta_{n-n'} \\
&\qquad\quad + \sum_{n'\neq 0}[\mathcal{G}(n,n') + \mathrm{Re}\mathcal{I}(n,n')]\dot{\zeta}_{n'}\zeta_{n-n'} \\
&\qquad\quad + \mathrm{Re}\sum_{n'\neq 0}[\mathcal{G}(n,n')\ddot{\zeta}_{n'}\zeta_{n-n'} + \mathcal{J}(n,n')\dot{\zeta}_{n'}\dot{\zeta}_{n-n'}], \quad (23)
\end{aligned}$$

where $\Lambda(n) = (|n| - 1)\dot{R}/R - B|n|(n^2 - 1)/R^3$. The mode-coupling terms are given by

$$\mathcal{F}(n,n') = \frac{|n|}{R}\left\{\frac{\dot{R}}{R}\left[\frac{1}{2} - \mathrm{sgn}(nn')\right] - \frac{B}{R^3}\left[1 - \frac{n'}{2}(3n' + n)\right]\right\}, \quad (24)$$

$$\mathcal{G}(n,n') = \frac{1}{R}\left\{|n|[1 - \mathrm{sgn}(nn')] - 1\right\}, \quad (25)$$

$$\mathcal{H}(n,n') = |n|\frac{\dot{R}^2}{R^3}\left\{\left(\frac{|n|}{5} + 2\right)\mathrm{sgn}(nn') - 1 - \frac{|n'|}{5} - \frac{3}{5}\mathrm{sgn}(n'(n - n'))\right\}, \quad (26)$$

$$\mathcal{I}(n,n') = |n|\frac{\dot{R}}{R^2}\left\{\left(\frac{|n|}{5} - 1\right)\mathrm{sgn}(nn') + 1 - \frac{|n'|}{5} - \frac{6}{5}\mathrm{sgn}(n'(n - n')) - \mathrm{sgn}(n(n - n'))\right\}, \quad (27)$$

and

$$\mathcal{J}(n,n') = \frac{1}{R}\left\{\frac{3}{5}|n|[1 - \mathrm{sgn}(n'(n - n'))] - |n|\mathrm{sgn}(nn') - 1\right\}. \quad (28)$$

Here, lengths are rescaled by $L = R_0$ and velocities by $U = Q/2\pi R_0$. We mention that when $\mathrm{Re} = 0$ Eqs. (23)–(28) reproduce the results obtained in Ref. [12] for the problem without inertia. For instance, if $\mathrm{Re} = 0$, $\Lambda(n)$ represents the linear growth rate of the noninertial system. We have also verified that the radial geometry Eqs. (23)–(28) reduce to the corresponding rectangular geometry equations computed in Sec. II A [Eqs. (8)–(11)] if we take the "rectangular geometry limit." Specifically, $\mathcal{F} \to 0$, $\mathcal{G} \to G$, $\mathcal{H} \to 0$, $\mathcal{I} \to I$, and $\mathcal{J} \to J$. This limit operation can be better understood in the dimensional version of the expressions: after appropriate reintroduction of dimensions, it is obtained by setting $R \to \infty$ and $Q \to \infty$, such that $Q/(2\pi R) \equiv v_\infty$ and $n/R \equiv k$ remain constant. In dimensionless form the corresponding limit can be obtained by setting $R \to \infty$, and $\dot{R} \to 1$.

Before turning to the analysis of the impact of inertia on the finger tip splitting mechanism, we briefly comment on the first-order (in ζ) portion of the mode-coupling equation (23). In contrast to the equivalent expression obtained in Sec. II B for the rectangular flow configuration [Eq. (12)], in radial geometry we obtain a differential equation containing time dependent coefficients

$$\mathrm{Re}\ddot{\zeta}_n + \left[1 - \mathrm{Re}\frac{\dot{R}}{R}\left(\frac{|n|}{5} - 2\right)\right]\dot{\zeta}_n - \left[\Lambda(n) - \mathrm{Re}\frac{\dot{R}^2}{R^2}(|n| - 1)\right]\zeta_n = 0, \quad (29)$$

in view of the fact that $R = R(t)$. This creates an impediment to obtain simple, closed form analytical expressions for the linear growth of the radial flow system. However, in agreement with Ref. [19] we have also verified that at the linear level inertia acts to restrain the growth of the perturbation amplitudes, characterizing a stabilizing behavior. This information is pretty much what one can extract at the linear regime.

We proceed by targeting the unveiling of more interesting morphological issues related to the action of inertia at the onset of nonlinearity. While an analysis like the one performed in Sec. II C (which directly uses the concept of a finger tip function) is not possible in the radial case with inertia, we can still examine finger tip splitting related issues by considering the coupling of just two Fourier modes: the fundamental n, and its first harmonic $2n$.

Regarding this point, Fig. 5 illustrates a parametric plot expressing the behavior of the ratio a_{2n}/R relative to a_n/R as time advances, for the coupling between modes $n = 5$, and $2n = 10$. The initial perturbation amplitudes are $a_n(0) = 3.0 \times 10^{-3}$ and $a_{2n}(0) = 3.0 \times 10^{-4}$, such that $a_n(0) \gg a_{2n}(0)$. For the case $\mathrm{Re} = 0.1$ the initial conditions $\dot{a}_n(0)$ and $\dot{a}_{2n}(0)$ match those conditions at $\mathrm{Re} = 0$. This type of plot is convenient to compare the morphologies for the cases with and without inertia, since the ratio a_n/R is related to the average size and overall n-fold symmetry of the patterned structure, while

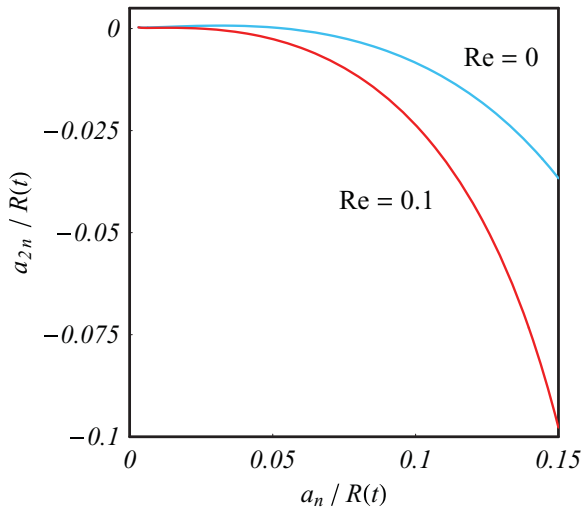

FIG. 5. (Color online) Behavior of $a_{2n}/R(t)$ with respect to $a_n/R(t)$ in the absence (Re = 0) and presence (Re = 0.1) of inertial effects.

a_{2n}/R determines the typical morphology of the finger tip (i.e., if the tips are wide and split, or if they are narrow and get sharper).

Situations involving both the absence (Re = 0), and the presence (Re = 0.1) of inertial effects are presented in Fig. 5 by considering a characteristic value for $B = 0.01$. It is clearly that as a_n/R is increased, a_{2n}/R tends to become more and more negative. Incidentally, this is the phase of the harmonic that favors finger tip widening and splitting. Furthermore, for any given value of a_n/R, it is apparent that when Re = 0.1 the ratio a_{2n}/R is more negative than for Re = 0. This observation suggests that, due to inertia, nonlinear effects naturally enhance tendency toward finger tip splitting.

Supplementary information about the role of inertial effects on the development of finger tip splitting events is provided by Fig. 6. It is nothing but the time evolution of the interfaces $[\mathcal{R}(\theta,t) = R(t) + a_0(t) + a_n(t)\cos(n\theta) + a_{2n}(t)\cos(2n\theta)]$ obtained by the perturbation amplitudes shown in Fig. 5, plotted at equal time intervals, assuming that Re = 0 for $0 \leqslant t \leqslant 12.5$ (left panel), and Re = 0.1 for $0 \leqslant t \leqslant 19.4$ (right panel). Notice that, the time evolutions cease when the same value of the ratio $a_n/R \approx 0.15$ is reached for both Reynolds numbers used.

We stress that the patterns on the left and right panels of Fig. 6 are not in scale. This is justified by the fact that, due to the stabilizing role of inertia, it takes a longer time to reach the prescribed condition for the ratio a_n/R. On the other hand, as seen in Fig. 6 the delayed fingers for Re = 0.1 will arise more bifurcated than those resulting from the equivalent evolution when Re = 0. Therefore, our weakly nonlinear results predict favored tip splitting behavior when inertia is taken into account.

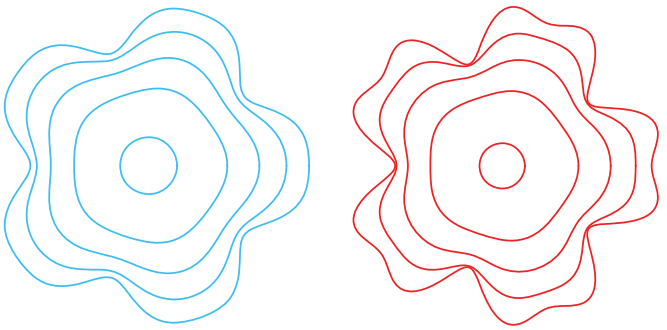

FIG. 6. (Color online) Snapshots of the evolving interface, plotted at equal time intervals for the interaction of two cosine modes $n = 5$ and $2n = 10$ when Re = 0 (left panel) and Re = 0.1 (right panel). Finger tip splitting is clearly favored on the right panel.

IV. CONCLUSION

By contrast to the great majority of studies of the Saffman-Taylor instability to date, recent experiments in rectangular Hele-Shaw flow [18], and a linear analysis in radial Hele-Shaw geometry [19], revealed that inertia can introduce important modifications on the stability and morphological aspects of the viscous fingering patterns. To examine further the influence of inertia on these systems, we approached the problem analytically by employing a mode coupling theory. The most advantageous and useful aspect of our theoretical model refers to its potential to capture inertially induced morphological changes already at lowest nonlinear perturbative order.

In agreement with previously reported linear stability results, we have verified that, for both flow geometries inertia acts to stabilize interfacial disturbances. Moreover, in line with existing experimental observations, we have found that increased inertia leads to the formation of wider fingers in rectangular channels. In the radial flow setup, despite the stabilizing nature of inertia at linear stages, we predict that finger tip splitting events are favored by the action of inertial effects. This enhanced bifurcation of the finger tips still needs to be checked by experiments.

On the theoretical side, a quantitative test of our chief analytic results to fully nonlinear stages of interface evolution would require the elaboration of numerical simulations capable of revealing inertial effects on convoluted patterns at advanced time regimes. Both boundary integral methods [21] and phase-field techniques [22] seem to be appropriate to effectively attack this long-time evolution problem.

ACKNOWLEDGMENTS

We thank CNPq for financial support through the program "Instituto Nacional de Ciência e Tecnologia de Fluidos Complexos (INCT-FCx)," and also through the CNPq/FAPESQ Pronex program.

[1] P. G. Saffman and G. I. Taylor, Proc. R. Soc. London A **245**, 312 (1958).
[2] G. M. Homsy, Annu. Rev. Fluid Mech. **19**, 271 (1987); K. V. McCloud and J. V. Maher, Phys. Rep. **260**, 139 (1995); J. Casademunt, Chaos **14**, 809 (2004).
[3] A. J. DeGregoria and L. W. Schwartz, J. Fluid Mech. **164**, 383 (1986).
[4] E. Meiburg and G. M. Homsy, Phys. Fluids **31**, 429 (1988).
[5] C.-W. Park and G. M. Homsy, Phys. Fluids **28**, 1583 (1985).

[6] P. Tabeling, G. Zocchi, and A. Libchaber, J. Fluid Mech. **177**, 67 (1987).
[7] T. Maxworthy, J. Fluid Mech. **177**, 207 (1987).
[8] J. A. Miranda and M. Widom, Int. J. Mod. Phys. B **12**, 931 (1998).
[9] L. Paterson, J. Fluid Mech. **113**, 513 (1981).
[10] S. N. Rauseo, P. D. Barnes, and J. V. Maher, Phys. Rev. A **35**, 1245 (1987).
[11] S. E. May and J. V. Maher, Phys. Rev. A **40**, 1723 (1989).
[12] J. A. Miranda and M. Widom, Physica D **120**, 315 (1998).
[13] O. Praud and H. L. Swinney, Phys. Rev. E **72**, 011406 (2005).
[14] S. W. Li, J. S. Lowengrub, J. Fontana, and P. Palffy-Muhoray, Phys. Rev. Lett. **102**, 174501 (2009).
[15] P. Gondret and M. Rabaud, Phys. Fluids **9**, 3267 (1997).
[16] C. Ruyer-Quil, C. R. Acad. Sci. Ser. IIb: Mec. **329**, 337 (2001).
[17] F. Plouraboue and E. J. Hinch, Phys. Fluids **14**, 922 (2002).
[18] C. Chevalier, M. Ben Amar, D. Bonn, and A. Lindner, J. Fluid Mech. **552**, 83 (2006).
[19] A. He and A. Belmonte, J. Fluid Mech. **668**, 436 (2011).
[20] E. O. Dias and J. A. Miranda, Phys. Rev. E **83**, 046311 (2011).
[21] S. W. Li, J. S. Lowengrub, and P. H. Leo, J. Comput. Phys. **225**, 554 (2007).
[22] R. Folch, E. Alvarez-Lacalle, J. Ortín, and J. Casademunt, Phys. Rev. E **80**, 056305 (2009).